Experimental Investigation on Structural Behavior of Continuous Concrete Beams Curved in Plan Reinforced with Cold-Formed Steel C-Section

Hayder. N. Al-Shibli¹, Mustafa B. Dawood², Ghalib M. Habeeb³

Ph.D. /University of Babylon/ Engineering Faculty/ alshiblihaider89@gmail.com Professor Mustafa B. Dawood eng.mustafa.balasum@uobabylon.edu.iq Professor Ghalib M. Habeeb Habeebghalib@yahoo.com

Abstract

This paper presents an experimental program on horizontally curved concrete beams reinforced with cold-formed steel C-section. Cold-formed steel sections are widely utilized in many construction fields as its low cost, light weight, eases manufacturing, reasonable force, erection and transportation. In some cases, increasing ultimate loading capacity with constant dimensions is needed for curved beams to resist high applied loads. Curved beams as compared to straight ones, are usually constructed with large width due to the high shear strength requirements. But in this study, transverse shear reinforcement with various configurations is introduced to improve a functional section with firm height and width for curved beams reinforced by cold-formed steel C-section. The experimental program is performed on curved in plan continuous concrete beam reinforced with a CFS C-section under two-point loading in which the ultimate loading strength, loaddeflection curve, and crack width are studied by replacing the traditional steel bars by a CFS C-section with openings, and with varying configuration of transverse reinforcement. In this research, reinforcing curved beam by a CFS section and the configurations of transverse shear reinforcement are the main studied variables. Transverse shear reinforcement with different arrangement are utilized, such as zig-zag, horizontal, vertical and inclined cross-stirrups shear reinforcement. Eight concrete curved beams were cast and tested under combination of two-point and continuing loading conditions. Depending on configuration of the transverse reinforcement, the experimental test outcomes indicated that introducing CFS C-section and transverse shear reinforcement increases ultimate loading strength of reinforced concrete curved in plan beam, enhances the deflection response and restricts the crack width for the same loading level.

Keywords: Reinforced concrete curved beam, Web opening, Horizontal stirrups, Vertical and horizontal stirrups, CFS stiffeners, Zig-zag stirrups, Inclined cross stirrups.

1 Introduction

Reinforced concrete curved in-plan beams are vastly utilized in many construction applications and it is also stated that curved in plan beams are more efficient than straight ones. In addition to the bending moment, horizontally curved beams are subjected to the torsional moment, and shear force under flexural status. Much research has been conducted to study behavior of RC curved in plan beams under diverse loading cases. Many variables that trace the performance of curved beams were specified, such as the material strength, reinforcing material and section, transverse reinforcing, web openings, curvature, and boundary conditions. The curved beam performance mainly relies on curvature in plan angle. In (2019) Numan et. al. [1], presented an experimental study four full-scale concrete reinforced curved beams. T-section was the cross-section for all specimens. Parametric study was conducted to examine the impact of concrete compressive strength and time casting segmental layers on the structural performance of such beams. Test results showed that the increase in the compressive strength of concrete for the flange zone increases significantly the ultimate capacity and reducing the deflection in the quarter span comparing with the control beam. In (2020) T. Xie et al. [2], presented an experimental and analytical program to investigate structural performance of ultra-high-performance fiber-reinforced concrete (UHPFRC) beams curved in plan under the act of concentrated loads subjected normally to the beam plane. 4 fixed-ends supported samples with subtended angles (curvatures) of 0°, 60°, 90°, and 120°, were tested. Structural responses, including rotation of out-of-plan, deflection, and the curved beams reactions under all loading stages, were studied experimentally. Test results appeared that by change in beam curvature, there was a change in beam mechanism of failure, ductility, and ultimate capacity of the beam decreased a bit with the increase in curvature. Also, test results showed that the materials under tension due to the strain-hardening performance of UHPFRC, there was an improvement in ultimate load and ductility over straight reinforced concrete beams. In addition, structural mechanics were developed for UHPFRC beams curved in plan using Castigliano's second theorem to portend the values of shear force, bending moment, torsional moment, and beam reactions under linear-elastic material statuses. Influence lines for shear force, torsional moment, and bending moment were also created using proofed equations of closed-form to demonstrate the effect of crucial variables on performance of UHPFRC beams. In (2020) Jayasheeri & Nethaji [3], reported

Vol: 2024 | Iss: 7 | 2024 | © 2024 Fuel Cells Bulletin 77

an experimental program on performance of horizontally curved RC beam under combined conditions of fixed axial loading and flexural in which the load-deflection of curved in plan reinforced concrete beams is investigated by varying the ratio of span/depth with constant beneath. Also, the influence of transverse shear reinforcement on flexural performance of curved in plan RC beam is examined for vary depth. As compared to straight beams, curved beams are constructed with large width due to the high shear strength requirements. But in their study, transverse shear reinforcement is introduced with various arrangements to develop an efficient section with fixed beneath. Vertical, horizontal, spiral, and zig-zag techniques were the transverse shear reinforcements used kinds. 6 groups of curved in plan RC beams were cast and tested under fixed axial loading and two-point loading status. Test results showed that submitting shear reinforcement in spiral and horizontal configurations increases ultimate load of the curved in plan RC beams for smaller sections. In (2020) Lewan et. al. [4], introduced a paper pointed at showing the cold-formed steel section structural capability as a probable structural element in civil engineering and building constructions. Authors reported some related studies in their paper that shows the possibility of using the cold-formed steel section as a structural member in the construction fields. As a results of the reported studies, by using a cold-formed steel section there was an increase in flexural capacities. Ultimately, and based on reported works, there was a possibility to utilize the cold-formed steel section as a probable structural element in light-weight constructions, small and medium size buildings, and in civil engineering applications. In (2021) W. H. Khaleel et al. [5], submitted a review paper on some previous theoretical and experimental studies about the reinforced concrete curved in plan or ring beams, strength, and behavior. Due to the curvature, there was a demand to include the effect of torsional forces in analysis & design. The most efficient variables worth reviewing are; the support number, ring diameter, concrete compressive strength, the width of the beam, and the bearing plate width. In addition to the finite element analysis, there are various methods of analysis to estimate the behavior and loading capacity. From the previous studies, increasing the ring diameter led to a decrease in the load capacity, while increasing the width of the beam, supports number, bearing plate width, and compressive strength of concrete increased the loading capacity. Reinforced concrete ring beams failed in flexure, as a failure as straight beams, deep ring beams failed in shear. Strut and tie model (STM) and plastic analysis are useful methods to analyze effectively ring-deep or curved beams. Moreover, non-linear FEM is idealistic for simulating the performance of RC curved in plan deep beams. In (2021) Abou Rayan et al. [6], made an experimental work on flexural performance of encased FCFS (flat cold-formed steel sections) and PCFS (perforated cold-formed steel sections). 11 samples were fabricated, cast, and tested up to failure. The control beam was tested without CFS section. 6 samples with FCFS were tested to explore the location influence and section area. The remaining four beams with a new shape of PCFS sections were tested at various locations. The main variables investigated and studied were CFS section position & elevation, and flange beneath. The ultimate strength and load-deflection curves were tested and recorded. Also, tested beams mode of failure were studied. Test outcomes indicated that there was an important increment in ultimate strength and stiffness of the composite samples with PCFS sections due to the position of CFS, the CFS top-flange width, CFS depth, and technique of connecting the concrete, stirrups, and cold-formed sections. In (2021) Kouider et. al. [7], reported a numerical & theorical study on performance of a large-span cold-formed steel beam with various webs (triangular corrugated, solid, and a trapezoidal corrugated). These beams are tested at mid-span under flexural concentrated force. ABAQUS finite element program was used to create the model. The analytical results obtained based on Eurocode 3 were used to evaluate the numerical results. The beam ultimate load and modes of failure were discussed. Corrugated web beams proceed better than all other sections according to analytical and numerical analysis. In (2021) Elsawaf &Bamaga [8], presented a numerical study on the composite action between the cold-formed steel (CFS) beams and the normal concrete. The 3-D brick components were utilized to design the numerical model to gain overall structural performance. The numerical outcomes were correlated to an eight specimens experimental outcomes, utilizing three kinds of newly shear connectors in addition to standard headed-stud shear-connectors, with 2 various of a CFS channel beam thickness. There was a good a agreement in performance of the shear connectors and modes of failure between the proposed numerical model and experimental one to expand composite action between concrete and CFS beam using the concrete-damaged plasticity model. In (2022) Witwit & Jasim [9], conducted an experimental and finite element analysis to examine structural performance of a new composite RC curved in plan beam, in which the connection between the reinforced concrete beams and the T-sections is proposed by utilizing the vertical reinforcement bars (stirrups) as shear connectors by passing them through perforated holes in the T-section web. Four specimens were reinforced as composite beams, cast, and tested under the combined effect of shear, bending, and torsion forces in addition to one conventional reinforced concrete curved in-plan beam as control. The utilized number of stirrups as shear connectors (which is considered as the degree of shear connection) varies for the fourth beams. Experimental investigations illustrated that the stirrups are very influential in stocking the interaction between the beam components. Also, there is no significant effect of shear connection degree on tested beams performance. ABAQUS was conducted to simulate the behavior of such beams. The numerical results showed an acceptable coincide

Vol: 2024 | Iss: 7 | 2024 | © 2024 Fuel Cells Bulletin

between the experimental and finite element results. In (2023) A. Rajić et al. [10], presented the possible analytical methods and a parametric numerical simulation study of cold-formed steel-reinforced concrete composite beams in flexure. Analyzed beams are conducted on the back-to-back cold-formed steel sections and concrete slabs fastened by demountable shear connectors. The solid concrete slab was analyzed on a metal sheet. In addition, studying the influence of corrugated web within the back-to-back channels of various thicknesses. The distance between the shear connectors is increased for the corrugated web. Moreover, shear connector quality, different degrees of shear connection, and their configurations are considered. The analytical study showed that the thickness of the steel channel, bolt arrangement & quantity, the degree of shear connection, and corrugated web affected significantly the beam bending capacity as well as the concrete slab arrangements. On the contrary, an unattached connection between steel elements has a small influence. Also, there is an acceptable match between the analytical approaches and FEM analysis outcomes.

From previous studies, it can be notice that there is a gap in studying the structural performance of horizontally curved beam reinforced by CFS section. This study is conducted to investigate the structural behavior of such beams.

2. Research Significance

Nowadays, there is a trend of using CFS section as reinforcing material in structural elements due to its advantages. In addition to curved structural members which preferred by architect for modern structures. Many researches have been conducted to study the structural behavior of straight RC beams incased CFS section, but there are no researches on the curved beams encased CFS section. This present experimental work is carried out on the horizontally curved beams reinforced by CFS section provided with different types of shear reinforcement in both vertical and horizontal direction. Also, developing an efficient section with constant dimensions to resist the applying loads, decreasing deflection and enhance other structural criteria of the horizontally curved continuous beams reinforced by cold-formed steel section.

3. Experimental programs

3.1 Tested beams

8 specimens were cast and tested to find out structural performance of curved in plan continuous concrete beams reinforced with CFS C-section. Each beam has a length of 2426 mm with an effective span of 2226 mm. The beam's cross-section was rectangular with 150*250 mm. The cross-section of reinforced concrete beams was designed to be able to resist a positive (sagging) bending moment of 14.5 kN.m, a negative (hogging) bending moment of 28.5 kN.m, a shearing force of 75 kN and a twisting moment of 3.5 kN.m. These values of the applied moments and forces were determined by applying a load of 200 kN on the whole beam, 100 kN for each span concentrated at the middle of the horizontally circular curved beam with a 1588 mm radius. Table 1 shows the details of the control specimen reinforced by steel bars and the other seven ones reinforced by C section with different transverse shear reinforcement, Figure 1 and Figure 2 show the description of the control and the C cross-section beams respectively, and Figure 3 illustrated specimens description.

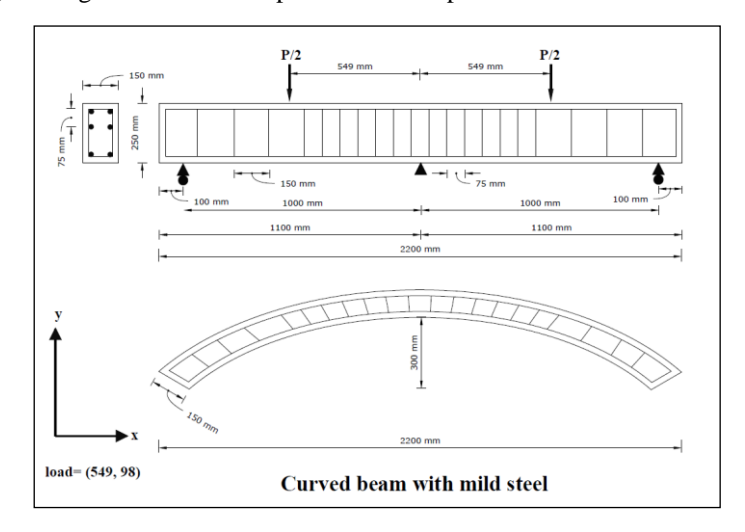
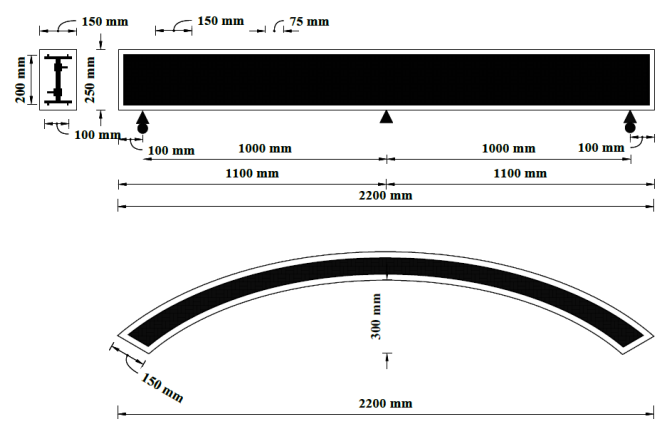


Figure 1 Description of the control beam



Curved beam with C cross-section

Figure 2 Description of the C cross-section beams

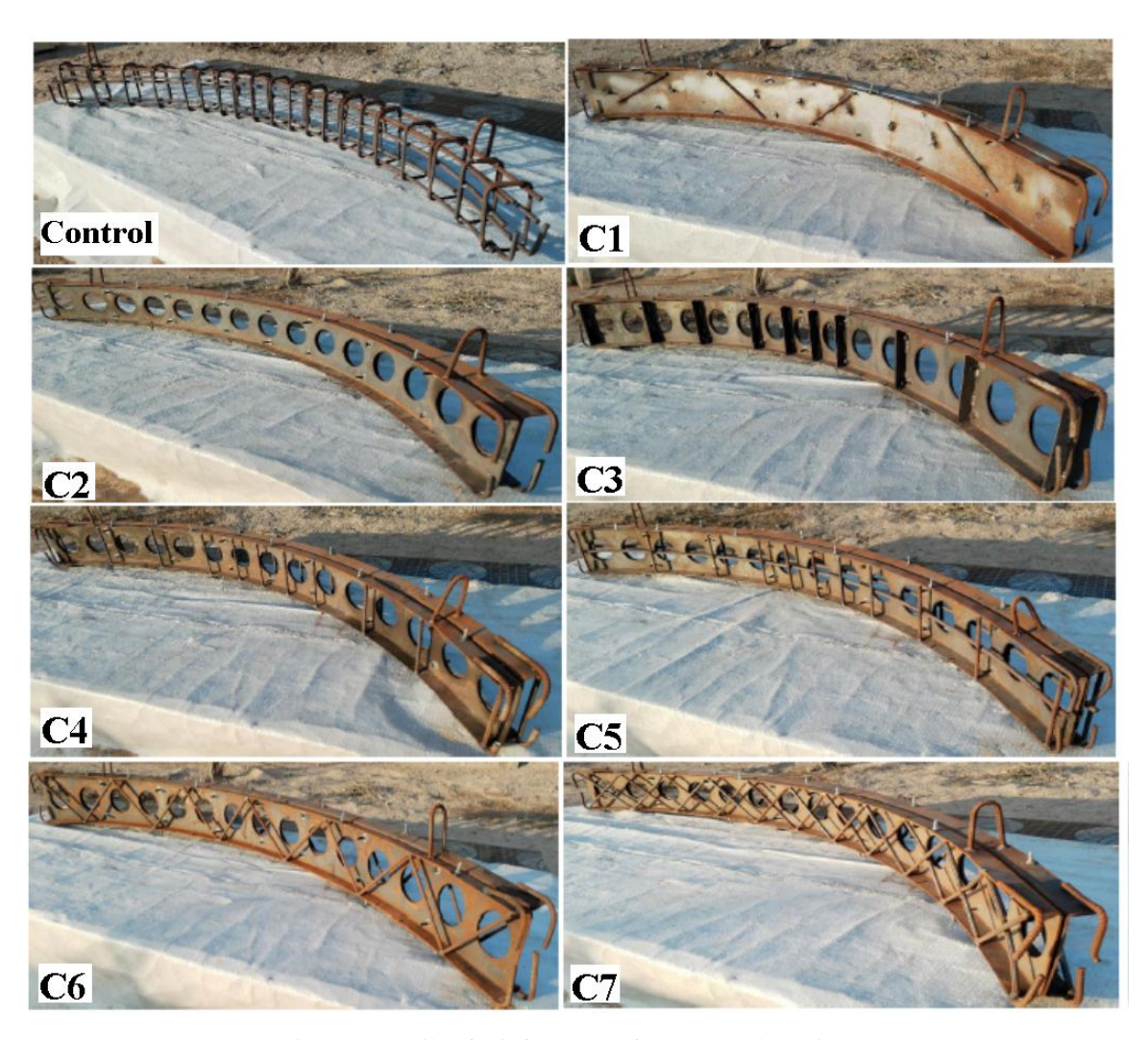


Figure 3 Details of reinforcement for the tested specimens

Table 1 Description of the tested specimens

Specimen symbol	Reinforcing	Configuration		
Control	Steel bars	Ordinary reinforcing		
C1	Cold-formed steel section	Only CFS		
C2	Cold-formed steel section	CFS with openings		
C3	Cold-formed steel section	CFS with openings with CFS stiffeners		
C4	Cold-formed steel section	CFS with openings with vertical stirrups		
C5	Cold-formed steel section	CFS with openings with horizontal& vertical stirrups		
C6	Cold-formed steel section	CFS with openings with inclined stirrups(zig-zag)		
C7	Cold-formed steel section	CFS with openings with cross-inclined stirrups		

3.2 Materials

The used cement was (Type 1) which is an ordinary cement that was conforming to Iraqi Specification (I.O.S 5/1984) [11]. The physical properties of the used cement are presented in Table 2.

Table 2 Physical Analysis of the Cement

Physical property		Test result	Iraqi Specification (I.O.S 45/1984)
Compressive strength	(3-day N/mm ²)	21	≥ 15
compressive stronger	(28-day N/mm ²)	28	≥23

This work adopted the steel reinforcement of (\emptyset 12) and (\emptyset 10) bars. Table 3 shows the material properties of the steel reinforcement used according to American Standard ASTM A615/A615M—2020.

Table 3 Material Properties of the Steel Reinforcement

Bar diameter (mm)	Yield strength (MPa)	Ultimate strength (MPa)	Modulus of elasticity (MPa)	Elongation (%)
12	510	724	200000	20.33
10	450	566	200000	21.68

All specimens were cast with normal-weight concrete with a designed compressive strength of 25 Mpa. The designed mix was 1:1.5:3 (by weight) cement, sand, gravel, and 0.4 water-cement ratio (w/c). A mixture was conducted to meet the requirements of the normal-weight concrete. The mix was designed according to the ACI (211-1) [12]. Table 4 lists the quantities of the final mix materials per cubic meter.

Table 4 Plan Concrete Mix Proportion

Material	Cement (kg/m³)	Coarse Aggregate (kg/m³)	Fine Aggregate (kg/m³)	Water (1/m³)	w/c
Amount	383	1120	675	150	0.4

A cold-formed steel sheet of 3.7 mm thickness was used to fabricate the cross-section to reinforce the beam. The cross-sectional area of the cold-formed steel was calculated by qualifying the force of mild steel with the force of CFS, as follows:

Force of mild steel = Force of CFS

(A* Yield strength) = (A* Yield strength)

The mechanical properties were tested according to the requirements of the ASTM A283 [13]. Tensile tests on 2 samples for each sheet were carried out, the tensile properties results are shown in Table 5.

Material	Thickness (mm)	Yield stress Fy (Mpa)	Ultimate stress Fy (Mpa)	Elongation (%)
CFS	3.7	325	468	11.32

Table 5 Properties of cold-formed steel

4. Test setup

All specimens were tested as continuous (two-spans) horizontally curved beams using a two-point load. The beams were tested by using a calibrated electrohydraulic testing machine with a maximum capacity of 2000 kN in the structure of the laboratory of Kufa University. The beams test was done under monotonically load increments and up to the failure. The beam was loaded at the upper face by vertical load, and then the first reading of the mechanical dial gauge was recorded. The load was applied at a constant rate on the specimen beams and gradually increased up to the failure. For each stage of load increment of load, the reading of the mechanical deflection (vertical displacement) in the mid-span of the beam was recorded. In addition, for each step of load, the crack patterns were checked, and the load of the first crack and failure of the beam were recorded. Figure 4 shows the setup for testing specimens and devices.

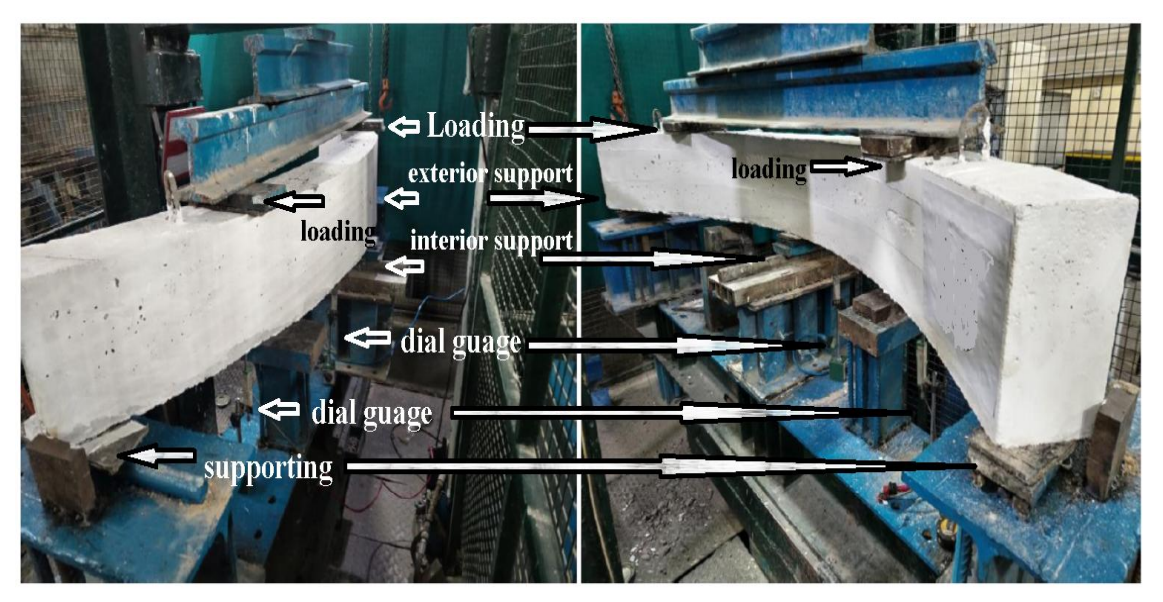


Figure 4 Testing specimen and device setup

5. Experimental Results and Discussion

This work was dedicated to studying the effect of combined forces of shear, bending, and torsion on the performance of the new proposed composite reinforced concrete beams curved in plan. Cold-formed steel section, stirrups configuration, and cold-formed steel stiffeners were the main parameters chosen to assess their effect on the performance of such beams. Eight specimens were tested to explore performance of curved in plan continuous concrete beams reinforced with cold-formed steel C-section, one of them was conducted to be the control beam under certain loading. The experimental results include ultimate strength, crack pattern, load-deflection curve, and failure mode. All eight specimens test results were summarized in Table 6

below, its observed that all specimens had an increase in carrying load capacity compared with the control beam. C5 and C7 specimens i.e., the specimen with CFS section stiffening with horizontal and vertical stirrups, and the specimen with inclined cross stirrups with increasing percentages of 84.9% and 100% respectively, were the most effective specimens in strength compared with the control beam. The C1 specimen had the least increase in ultimate strength compared with the control specimen, the increment was about 46.7%. From the test results, it can be observed there is an improvement in structural criteria's as ultimate strength, deflection response, crack width, and failure mode.

Ultimate load increment Max. deflection First crack Ultimate Service load Beam symbol load (kN) ratio (%) (mm) at center load (kN) (kN) 225 150 Control 4.21 60 C₁ 46.7 70 330 221.1 4.82 C2 337 49.8 225.79 5.43 90 C3 370 64.4 247.9 5.85 70 C4 345 231.15 53.3 7.46 80 C5 416 84.9 278.72 9.72 70 375 66.7 251.25 7.12 120 C6 C7 450 100 301.5 11.25 120

Table 6 Results summary of the tested beams

5.1 load-deflection response

In general, there are three levels of response for specimens: elastic un-cracked, elastic cracked, and ultimate stages, the first level ends when cracks are initiated.

At the uncracked stage, the deflection starts with a steep slope linearly in all specimens during the loading process, due to the material's elasticity feature in the tension and compression zones. When the cracking began, the load-deflection curve stayed linearly but with a slope steeper than the previous (uncracked) stage. At the latter level, the load-deflection slope decreased largely up to failure with a slight load increment for some specimens. While the other specimens' load-deflection slope becomes more rise upward, this behavior may be referred to as the contribution of the cold-formed steel section in resisting and reducing the deflection magnitude. The load-deflection curves of the tested specimens are shown in Figure 5 below.

From Figure 5 below, there is a clear enhancement in the load-deflection curve of specimen C-1 compared with the control one for the same loading level. A match was found between specimen C-2 and the control beam. There is an enhancement in the load-deflection curve for specimen C-3 until the cracking level, after this level, the two curves slope of these specimens became identical. For the curves of the other specimens, there is a relative match between them and the control one until the advanced loading level, their slopes become more sleeper compared with the control.

This variation between the load-deflection curves of the tested specimens referred to using cold-formed steel sections and the configuration of stirrups.

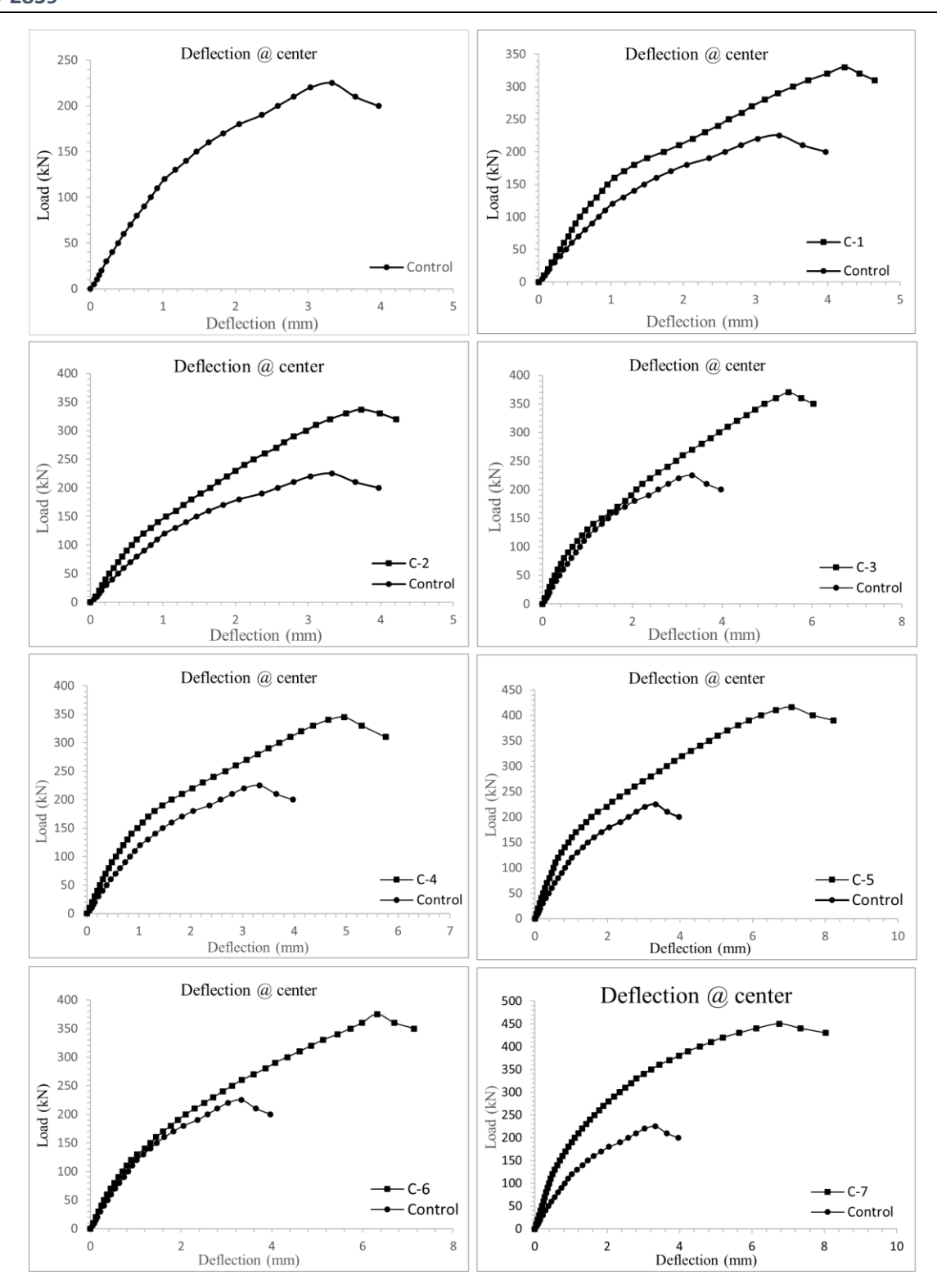


Figure 5 Load-deflection curves of tested specimens

5.2 Modes of failure

Four types of cracks have been formed, diagonal shear cracks, flexural cracks, flexural-shear cracks, and torsional-shear cracks. As shown in experienced specimens, the flexural cracks formed at beam top face above interior support where the maximum negative (hogging) moment and under the loading point at the bottom face of the midspan where the positive (sagging) moment, torsional-shear cracks formed diagonally between loading and supporting points, and diagonal cracks formed between the loading and interior supporting points caused failure for some specimens. Crushing of concrete happened at loading and supporting points for most specimens.

Due to using the CFS section, there is an important increment in loading carrying capacity in all specimens, accompanied by a reduction in cracks and enhancement in deflection response for the same loading level. The cracks reduction and restriction in their formation may be referred to using stiffeners and stirrups configurations that cut cracks path formation leading to more resistance in carrying load.

As shown in Figure 6 below, the control and C-4 specimens, failed with major shear cracks with concrete crushing. A major shear crack, torsional cracks, and concrete crushing in loading points caused failure for specimen C-1. The specimens C-2 and C-3 failed with torsional crack accompanied by concrete crushing. C-5 failed with a torsional-flexural crack accompanied by the crushing of concrete in loading & supporting points. Crushing of concrete in loading points and a diagonal shear crack caused a failure for specimen C-6. A failure of specimen C-7 was caused by a major shear crack, flexural crack, and crushing of concrete in loading & supporting points.



Continued



Figure 6 Modes of failure for tested beams

5.3 Ductility

Ductility can be defined as the ability to maintain inelastic deformations without losing the ability to carry a load before failure. The current work examines ductility variables by dividing vertical displacement at maximum load by vertical displacement at service load [14]. All specimens exhibit an increase in ductility. The ductility factors of tested samples are listed in Table 7 below. Ductility index can be expressed as the ((specimen ductility- control ductility)/ control ductility).

Table 7 Ductility factor for tested specimens

Specimen	Service deflection, Δs (mm)	Max. deflection@ center, Δu (mm)	Ductility factor μ ($\frac{\Delta u}{\Delta s}$)	$\left(\frac{\mu_i - \mu_r}{\mu_r}\right) * 100 \%$
Control	3.4	4.21	1.24	_
C-1	2.89	4.82	1.67	34.68
C-2	3.94	5.43	1.38	11.29
C-3	4.43	5.85	1.32	6.45
C-4	5.4	7.46	1.38	11.29
C-5	7.26	9.72	1.34	8.1
C-6	4.44	7.12	1.6	29.03
C-7	6.98	11.25	1.61	29.83

 $P_{\text{service}} = 0.65 * P_{\text{ult.}} \text{ (Jeffrey, 2003)}$

 μ_r = Control ductility

 μ_i = Specimen ductility

5.4 Stiffness criteria

The stiffness basically can be defined as the material resistance against deflection or deformation or the loading needed to produce unit deflection in the member i.e. [(0.75*Pmax.) / (deflection @ 0.75*Pult.)] (Muthuswamy & Thirugnanam, 2014) [15]. The material with lesser deformation or deflection will have more strength and stiffness as a result. There was an enhancement in stiffness for specimens C-1 C-2, C-3, C-4, and C-6, while there was a degradation in the stiffness of specimens C-5, and C-7. Stiffness values for tested specimens are listed in Table 8 below. Stiffness index can be expressed as the percentage of ((specimen stiffness-control stiffness)/ control stiffness).

Table 8 Stiffness values for tested specimens

specimen	0.75 P _{ult.} (kN)	Deflection vs 0.75 P _{ult.} (mm)	Stiffness, κ (kN/mm)	$(\frac{\kappa_{\rm i} - \kappa_{\rm r}}{\kappa_{\rm r}}) * 100 \%$
Control	169	3.64	46.43	_
C-1	247.5	3.22	76.86	65.54
C-2	252.75	4.13	61.2	31.81
C-3	277.5	3.65	76.03	63.75
C-4	258.75	5.05	51.24	10.36
C-5	312	7.93	39.34	-15.27
C-6	281.25	5.08	55.36	19.23
C-7	337.5	8.36	40.37	-13.05

 κ_r = Control stiffness

 κ_i = Specimen stiffness.

5.5 Summary of test results of the curved continuous beams

Figure 7 shows a comparison of load deflection at the center of a span, Figure 8 shows a comparison of shear cracking loads, and Figure 9 shows a comparison of flexural cracking loads. It can be seen clearly that all specimens exhibited an increase in ultimate loading capacity, enhancement in load-deflection response, increase in the first cracking load for both shear and flexural, and decrease in crack width for the same loading level compared with the control specimen. Also, one can

observe the great enhancement in ultimate loading capacity and deflection response for specimen C-7 compared with the other specimens.

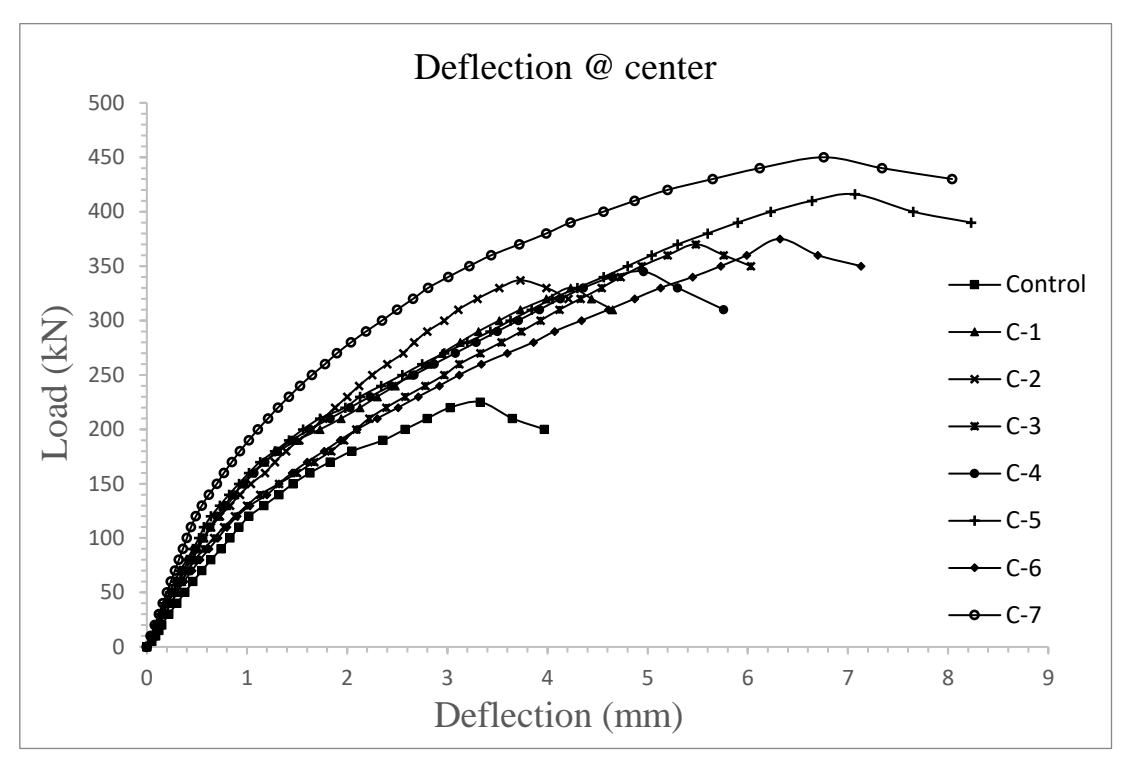


Figure 7 A comparison of load deflection at the center of one span

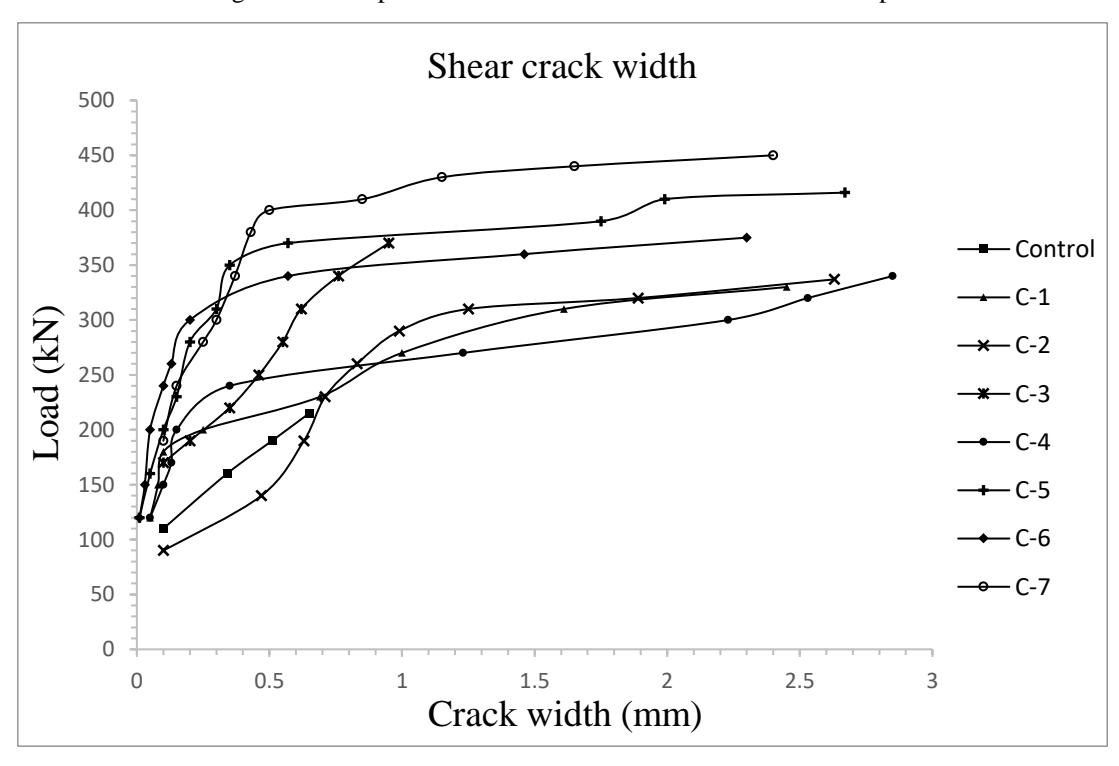


Figure 8 A comparison of the shear cracking load

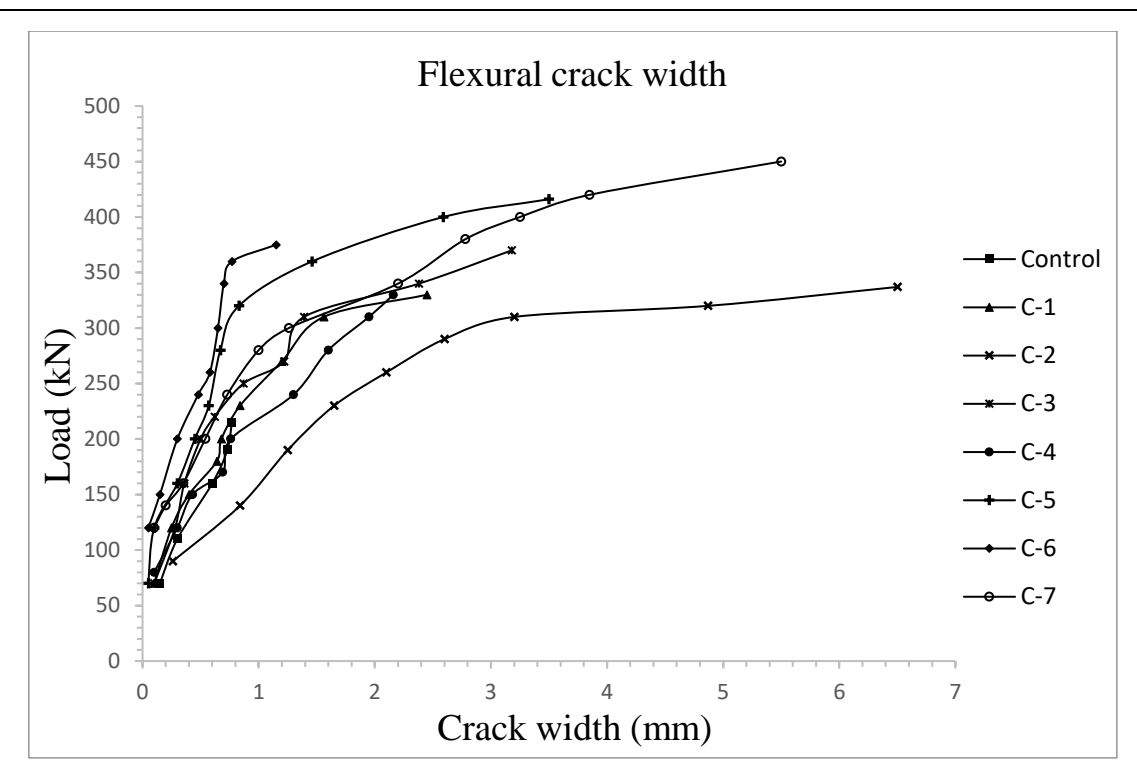


Figure 9 A comparison of the flexural cracking load

6. Conclusions

The Conclusions marked from investigation levels (experimental analysis) for horizontally curved continuous concrete beam reinforced with I-cold formed steel section, reinforced with different configurations of transverse steel bars:

- 1. Replacing the cold-formed steel section instead of mild steel led to a significant increment in carrying load capacity for the same section.
- 2. Using stiffeners increases strength and decreases deflection and cracking load for most specimens at the same loading stage.
- 3. The C-section with cross-inclined stirrups (specimen C-7) was the most powerful section in terms of load capacity and decreasing deflection.
- 4. The presence of openings was for bonding and there is a negligible effective contribution to loading capacity.
- 5. Cold-formed steel stiffeners significantly increase carrying load but increase deflection more than the other specimens.

References

- [1] Numan, H. A., Waryosh, W. A., & Ali, S. S. (2019). Behavior of Laminated Reinforced Concrete Curved Beam with Changing Concrete Properties. *Civil Engineering Journal (Iran)*, 5(2), 284–294. https://doi.org/10.28991/cej-2019-03091244.
- [2] Xie, T., Mohamed Ali, M. S., Elchalakani, M., & David, M. (2020). Experimental and Analytical Study of Ultrahigh-Performance Fiber-Reinforced Concrete Curved Beams. *Journal of Structural Engineering*, 146(2). https://doi.org/10.1061/(asce)st.1943-541x.0002502.
- [3] Nethaji, M. (2020). Experimental Investigation on Flexural Behavior of Reinforced Concrete Curved Beams with different Types of Shear Reinforcement. *Jeyashree & Nethaji International Journal on Emerging Technologies*, 11(3), 615–618. www.researchtrend.net.
- [4] Lawan, M. M., Shek, P. N., & Tahir, M. M. (2020). Can Cold-Formed Steel Section Be Use As A Sustainable Structural Member in Building and Civil Engineering Constructions? A Mini Review. *IOP Conference Series: Materials Science and Engineering*, 884(1). https://doi.org/10.1088/1757-899X/884/1/012039.

- [5] Khaleel, W. H., Dawood, A. A., Abdul-Razzaq, K. S., Talal, A. A., & Al-Karawi, S. N. (2021). Reinforced Concrete Curved Beams in Literature. *IOP Conference Series: Materials Science and Engineering*, 1105(1), 012098. https://doi.org/10.1088/1757-899x/1105/1/012098.
- [6] Abou-Rayan, A., Khalil, N., Youssef, A., & Eldeib, M. (2021). Flexural Behavior of Encased Beam Flat or Perforated Steel Cold Formed Sections. *International Journal of Steel Structures*, 21(4), 1465–1477. https://doi.org/10.1007/s13296-021-00515-9.
- [7] Kouider, N., Hadidane, Y., & Benzerara, M. (2021). Numerical investigation of the cold-formed I-beams bending strength with different web shapes. *Frattura Ed Integrita Strutturale*, *16*(59), 153–171. https://doi.org/10.3221/IGF-ESIS.59.12.
- [8] Elsawaf, S. A., & Bamaga, S. O. (2021). Strength capacity and failure mode of shear connectors suitable for composite cold formed steel beams: Numerical study. *Materials*, *14*(13). https://doi.org/10.3390/ma14133627.
- [9] Witwit, D., & Jasim, N. (2022). Behaviour of New Curved in Plan Composite Reinforced Concrete Beams. *Basrah Journal for Engineering Science*, 22(2), 80–89. https://doi.org/10.33971/bjes.22.2.12.
- [10] Rajić, A., Lukačević, I., Skejić, D., & Ungureanu, V. (2023). Cold-formed Steel-Concrete Composite Beams with Back-to-Back Channel Sections in Bending. *Civil Engineering Journal (Iran)*, 9(10), 2345–2369. https://doi.org/10.28991/CEJ-2023-09-10-01.
- [11] Iraqi Specification No.5, "Portland Cement", Baghdad, 1984.
- [12] ACI 211.1 Standard Practice for Selecting Properties for Normal, Heavyweight, and Mass Concrete (ACI 211.9-91).
- [13] ASTM A283, "Standard Test Methods and Definitions for Mechanical Testing of Steel Products," ASTM International, 2004.
- [14] Russell, J. S. (2003). Prestrectives in Civil Engineering. Commemorating the 150th Anniversary of the American Society of Civil Engineering, ASCE Publications.
- [15] Muthuswamy, K. R., & Thirugnanam, G. S. (2014). Structural behaviour of hybrid fibre reinforced concrete exterior beam-column joint subjected to cyclic loading. International journal of civil and structural engineering, 4(3), 262–273. https://doi.org/10.6088/ijcser.201304010026.

APPENDIX A

ANALYSIS OF REINFORCED CONCRETE BEAMS

A.1Analytical Solution of Horizontally Curved Box Beam (Control Beam)

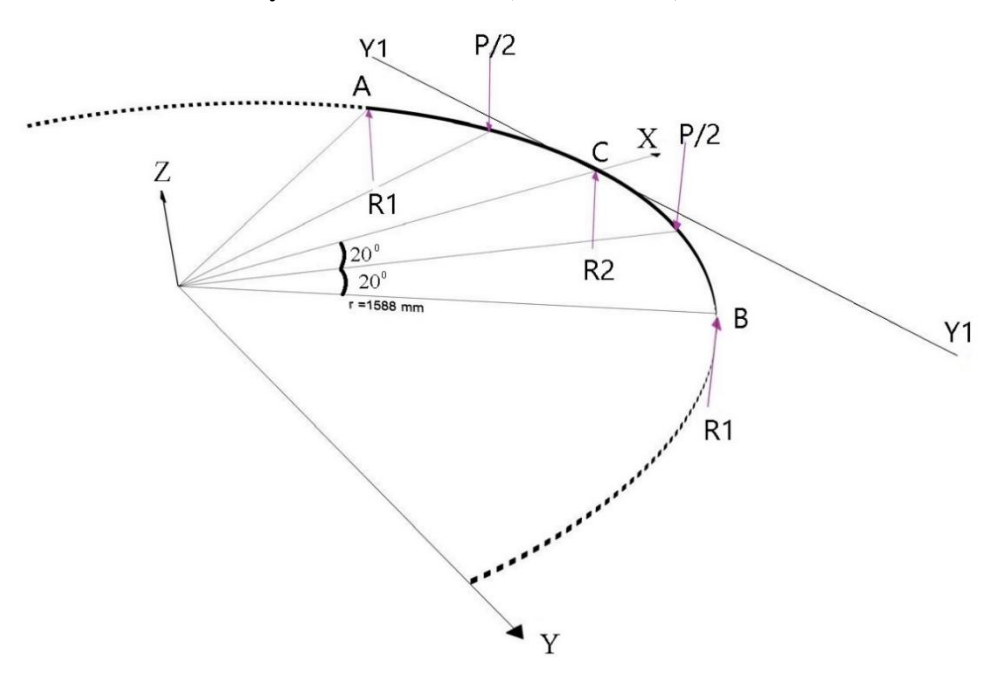


Figure A-1 Horizontally Curved Beam Loads and Forces

As in Figure A.1, the radius of the Horizontally Curved Beam = r = 1588 mm.

The applied load on each span =
$$\frac{P}{2}$$

Reaction at A = Reaction at B = R1

Reaction at C = R2

The Supports A &B are located at a distance of 375 mm from the Y1-Y1 axis and a distance of 1050 mm from the X-axis. The applied loads are located at a distance of 98 mm from the Y1-Y1 axis and a distance of 550 mm from the X-axis. Taking a moment of forces about the Y1-Y1 axis (through support C):

$$2* R1* 375 = 2* \frac{P}{2} * 98$$

$$R1 = 0.128 P = Ra = Rb$$

$$\Sigma Fy = 0$$

$$R2 = 0.872 P = Rc$$

By taking a section before and after the applied load we can find the shear, bending moment and torque equations.

• Shear, Moment, and Torsion calculation

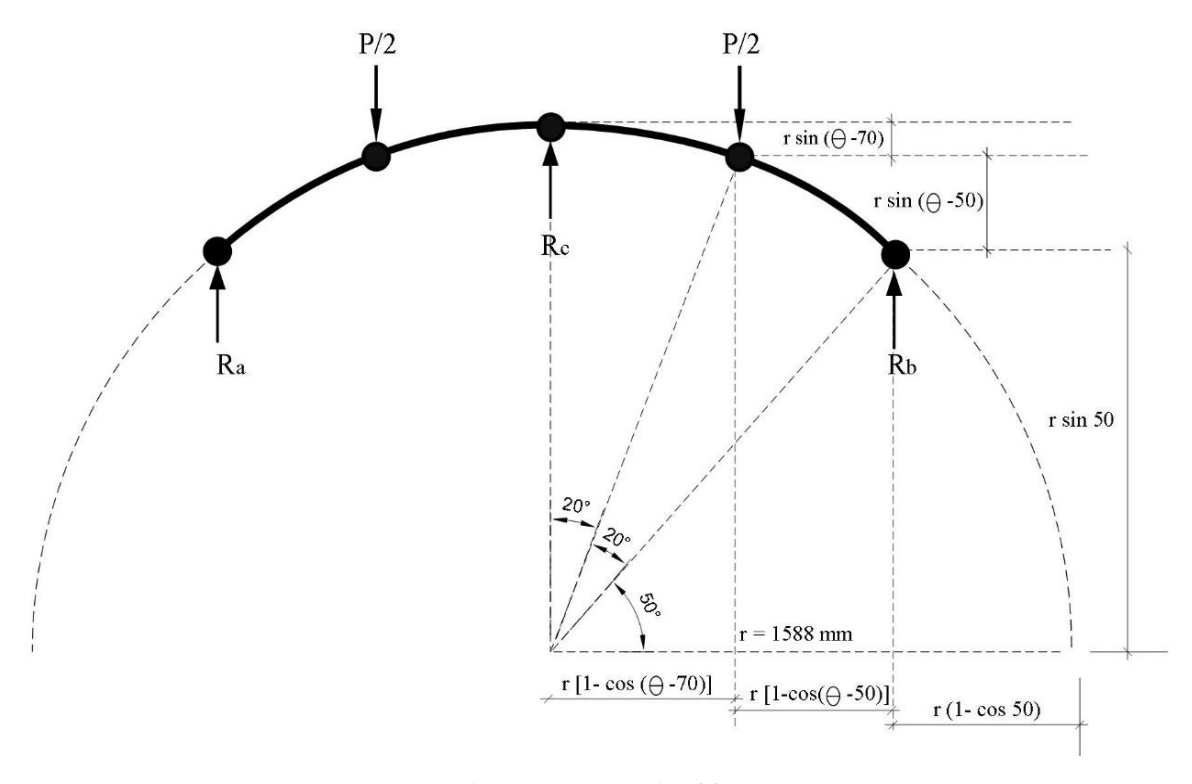


Figure A-2 Analysis of forces and loads

1. For $50^{\circ} < \theta < 70^{\circ}$

$$V = Rb = R1 = 0.128 P$$

$$M_{\theta} = 0.128 P * r * \sin (\theta - 50^{\circ})$$

$$T_{\theta} = 0.128 P *r8 [1 - \cos (\theta - 50^{\circ})]$$

2. For $70^{\circ} < \theta < 90^{\circ}$

$$V = R1 - 0.5 P = 0.128 P - 0.5 P = -0.372 P$$

$$M_{\theta}$$
 = 0.128 P * r * $\sin (\theta$ - 50°) – 0.5 P *r * $\sin (\theta$ -70°)

$$T_{\theta} = 0.128 \ P * r8 \ [1 - \cos (\theta - 50^{\circ})] - 0.5 \ P * r * [1 - \cos (\theta - 70^{\circ})]$$

Shear force diagram

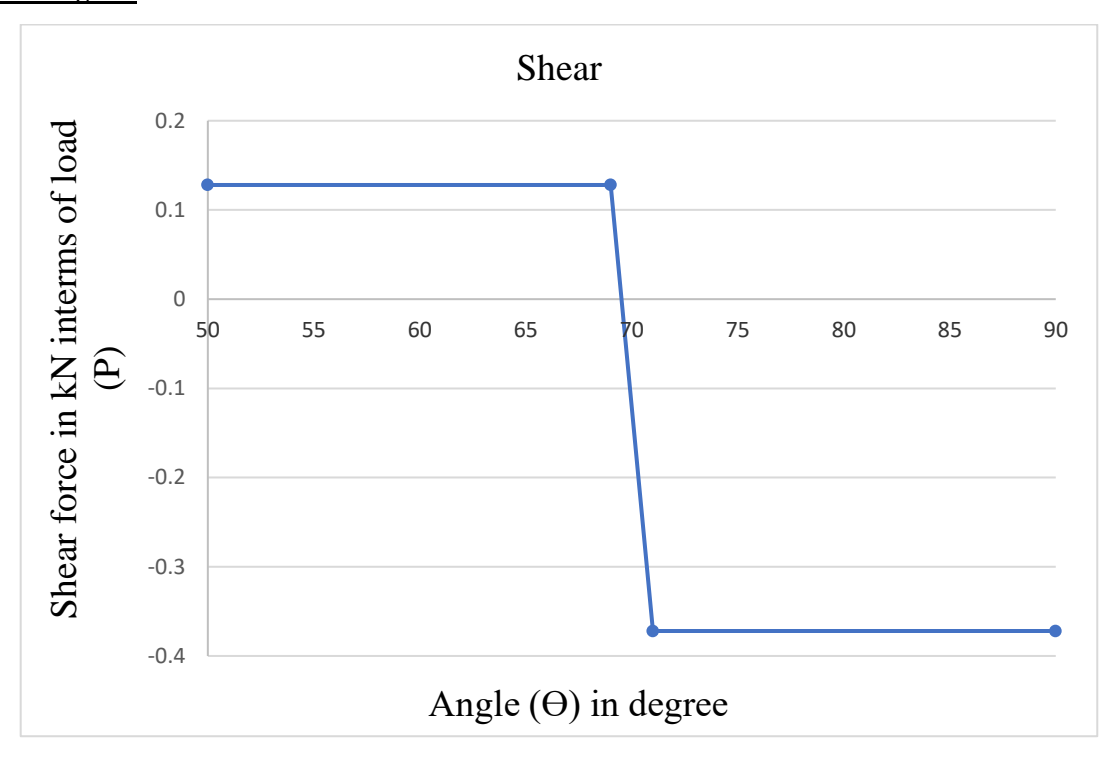


Figure A-3 Shear force diagram

Moment diagram

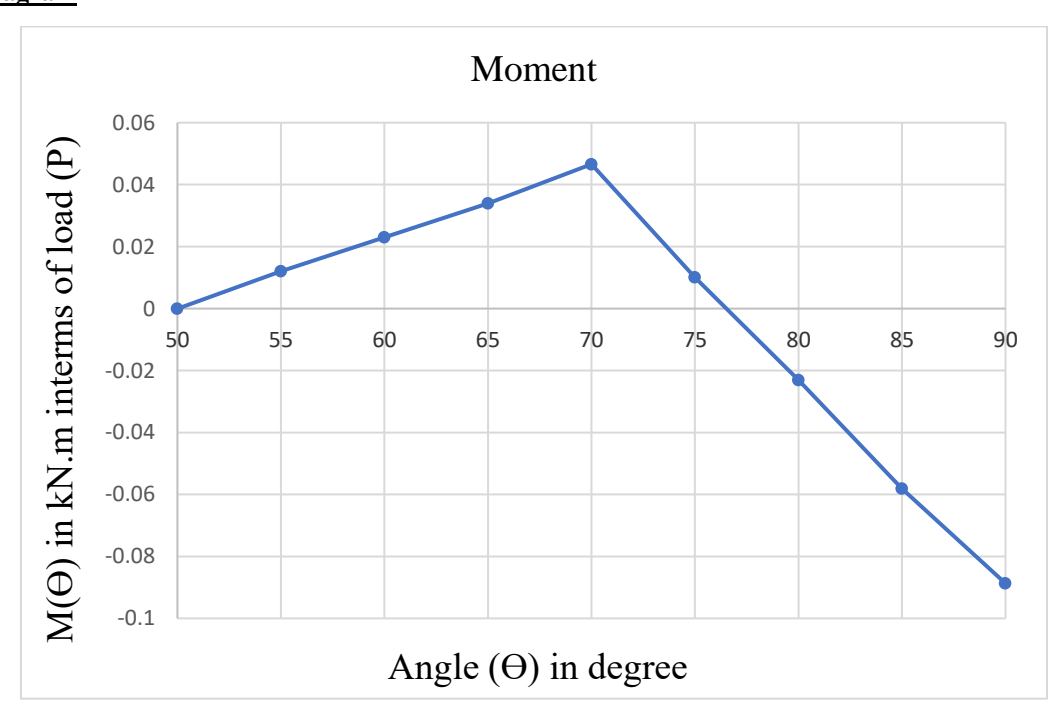


Figure A-4 Moment diagram

Torsion diagram

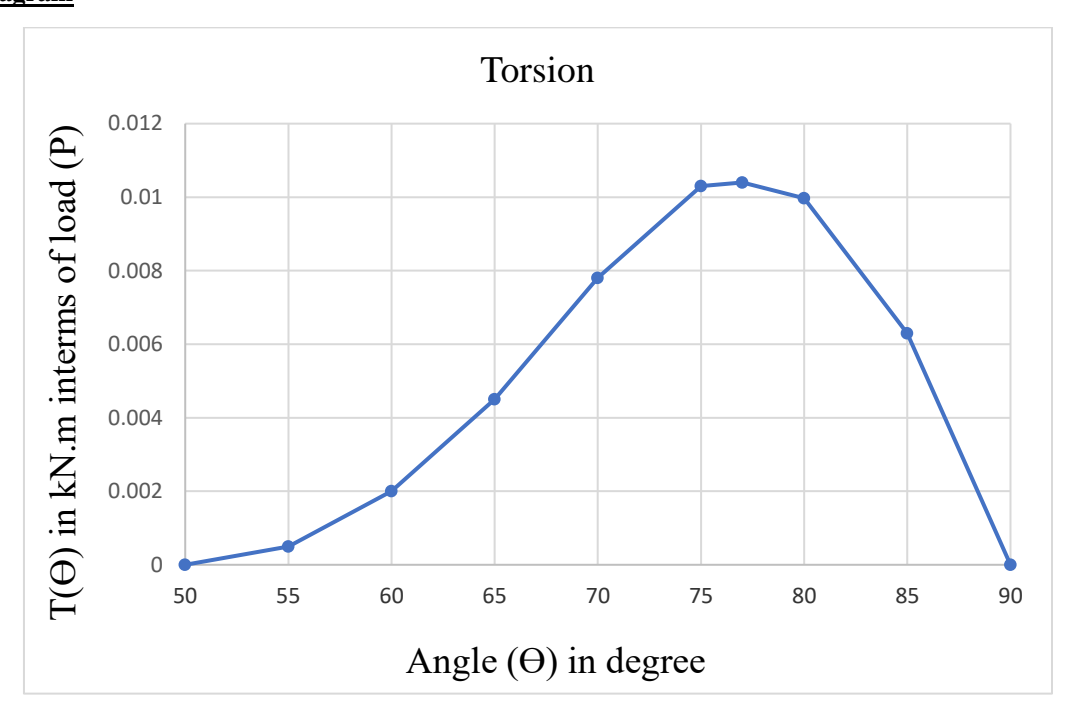


Figure A-5 Torsion diagram

A-2 Designing of the control beam

The applied load was chosen to be 200 kN, P = 200 kN

The material properties were as follows:

$$f'_c = 35 \text{ Mpa}$$

$$fy = 550 \text{ Mpa}$$

$$fy_t = 314 \text{ Mpa}$$

1. Positive moment

$$Mu^+ = 0.0446 * P* r$$

Mu⁺ =
$$\rho$$
.d². b. fy (1- 0.59. ρ . $\frac{fy}{f'c}$)

14.45*10⁶ =
$$\rho$$
. 225². 150. 420 (1- 0.59. ρ . $\frac{420}{25}$)

$$\rho_1 = 0.0961$$
 (neglected), $\rho_2 = 0.0045$ (ok)

$$\rho_{\text{max.}} = 0.85 * \beta 1 * \frac{fy}{f'c} * \frac{0.003}{0.003 + 0.005}, \beta 1 = 0.85 \text{ for } f'_{\text{c}} = 25 \text{ Mpa}$$

$$=0.85*\ 0.85*\ \frac{420}{25}*\frac{0.003}{0.003+0.005}=0.016$$

$$\rho_{\text{min.}} = \text{max. of } \left[\frac{\sqrt{fc}}{4fy} = \frac{\sqrt{25}}{4*420} = 0.0029, \frac{1.4}{fy} = \frac{1.4}{420} = 0.0033 \right]$$

ISSN: 1464-2859

$$\rho_{min.}=0.0033$$

$$\rho_{min.} < \rho = 0.00475 < \rho_{max.} \text{ okay}$$

$$As^{+} = \rho * b * d$$

$$= 0.00475*150*225 = 160.31 \text{ mm}^2$$

2. Negative moment

$$Mu^{-} = 0.0887* P* r$$

$$Mu^{-} = \rho.d^{2}$$
. b. fy (1-0.59. ρ . $\frac{fy}{f'c}$)

28.17*
$$10^6 = \rho$$
. 225². 150. 420 (1- 0.59. ρ . $\frac{420}{25}$)

$$\rho_1 = 0.0911$$
 (neglected), $\rho_2 = 0.00978$ (ok)

$$\rho_{min.} < \rho = 0.00978 < \rho_{max.} \ okay$$

$$As^-$$
 bending = ρ^* b^* d

$$= 0.00978*150*225 = 330.1 \text{ mm}^2$$

3. Shear plus torsion

$$T_{max} = 0.0104 * P* r$$

$$= 0.0104 * 200 * 1.588 = 3.303$$

$$V_{max.} = 0.372 * P = 0.372 * 200 = 74 \text{ kN}$$

According to the ACI-318 code provision, torsion may be neglected if it is less than:

$$\Phi$$
 (0.083) $\sqrt{\int C} \frac{Acp2}{Pcp}$, where A_{cp} = 250 *150= 3750 mm², P_{cp} = 2(250+150) = 800 mm

$$\lambda = 1$$
 normal concrete, $\Phi = 0.75$

$$0.75* \ (0.083) \ \sqrt{25} \ \frac{(3750)2}{800} * \ 10^{\text{-6}} = 0.547 \ kN.m < 3.303 \ kN.m$$

The torsion reinforcement is needed.

Hence, the section properties are calculated assuming the concrete cover is 25 mm and stirrups are 10 mm in diameter.

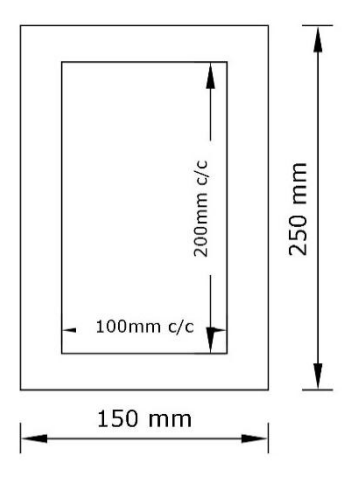


Figure A-6 Section dimensions for torsion calculation

 $x_1 = 100 \text{ mm c/c}$

 $y_1 = 200 \text{ mm c/c}$

$$A_{oh} = x_1 * y_1 = 100 * 200 = 20000 \ mm^2$$

$$A_o=0.85*A_{oh}=17000 \ mm^2$$

$$P_h=2*(x_1+y_1)=600 \ mm$$

$$V_C = \frac{\sqrt{f'c}}{6}$$
. b. d. $10^{-3} = \frac{\sqrt{25}}{6} * 150 * 225 * 10^{-3} = 28.125 \text{ kN}$

Checking if the section dimensions are satisfying eq. 22.7.71aof the ACI-318 code (2019) page 427:

$$\sqrt{\left(\frac{vu}{bw.d}\right)^2 + \left(\frac{Tu.Pn}{1.7*Aoh^2}\right)^2} \le \Phi\left(\frac{vc}{bw.d}\right) + 0.66\sqrt{f'c}$$

$$\sqrt{\big(\frac{74*10^3}{150*225}\big)^2 + \big(\frac{3.303*600*10^6}{1.7*2000^2}\big)^2} \leq 0.75 \left(\frac{28.125*10^3}{150*225}\right) + 0.66 \sqrt{25}$$

3.647 kN.m > 3.1 not ok

The transverse torsional reinforcement will be

$$\frac{A_t}{S} = \frac{T_n}{2 \text{ Aof } yt} = \frac{3.303*10^6}{2*17000*314} = 0.309 \text{ mm}^2 / \text{mm} \text{ for one leg}$$

The shear reinforcement is required because:

$$Vu = 74 > \frac{Vc}{2} = \frac{28.125}{2} = 14.06 \text{ kN}$$

: the shear reinforcement is required:

$$\frac{A_v}{S} = \frac{Vs}{fyt.d} = \frac{45.875 \times 10^3}{314 \times 225} = 0.649 \text{ mm}^2/\text{ mm for two legs}$$

Selecting stirrups

$$2*\frac{A_t}{S} + \frac{Av}{s} = 2*0.309 + 0.649 = 1.267 \text{ mm}^2/\text{mm}$$

Use $\emptyset 10 \ mm \ (As = 78.5 \ mm^2)$

$$S = \frac{2*78.5}{1.267} = 123.9$$

Checking:

Max. spacing
$$\frac{Ph}{8} = \frac{600}{8} = 75 \text{ mm or } 300 \text{ mm}$$

 \therefore use S= 75 mm c/c

Min. area of reinforcement for web:

$$A_v + 2A_t = \frac{1}{16} * \sqrt{\int C} b_w. d$$

= $\frac{1}{16} * \sqrt{25} * 150*225 = 10.55 \text{ mm}^2 < 2*78.5 = 157 \text{ mm}^2$

Longitudinal reinforcement is required if:

$$A_{l} = \frac{At}{s} * P_{h=0.309*600=185.4 \text{ mm}^2}$$

ACI- 318-19, 9.6.4.3 p138, state that if torsional reinforcement is required, the min. area of longitudinal reinforcement shall be lesser of:

a)
$$\frac{5*\sqrt{fc}*Acp}{fy}*-\left(\frac{At}{s}\right)P_h\left(\frac{fyt}{fy}\right)$$

$$\frac{5*\sqrt{25}*37500}{420}* - (0.309)*600* (\frac{314}{420})_{=2093.53}$$

b)
$$\frac{5*\sqrt{25}*37500}{420}* - \left(\frac{25\ bw}{fyt}\right)P_{h}\left(\frac{fyt}{fy}\right)$$

$$\frac{5*\sqrt{25}*37500}{420}* - \left(\frac{25*150}{314}\right)*600* \left(\frac{314}{420}\right) = -3125 \text{ mm}^2 \text{ (neg.)}$$

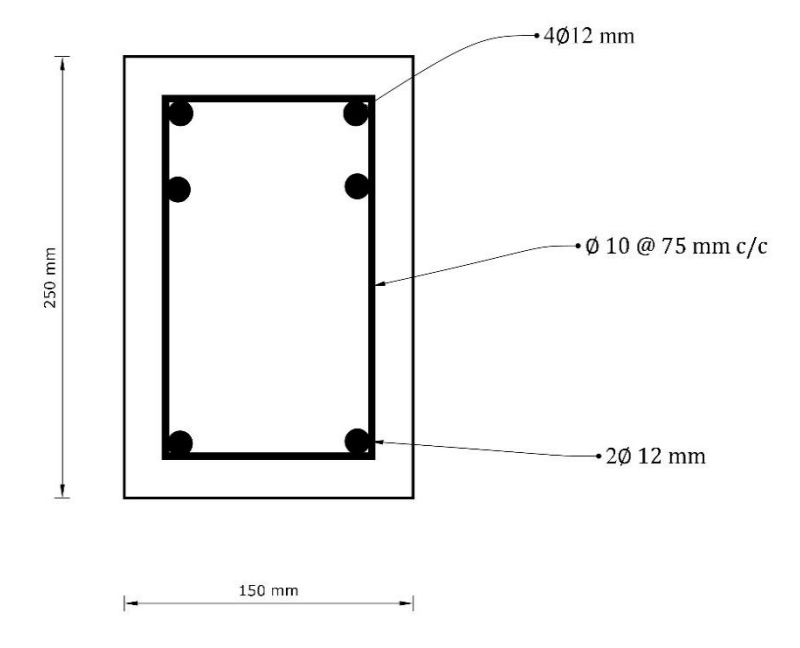
 A_l = 185.4 mm², to be divided into two layers (185.4/2 = 92.7 mm²), then added to the steel area as follows:

$$As^{+}= As_{bending} + A_{l}$$

$$= 160.31 + 92.7 = 253 \text{ mm}^{2}$$

$$As^{-}= As_{bending} + A_{l}$$

The final cross-section is



A.3 Cold-formed steel section calculation

A cold-formed steel sheet of 3.7 mm thickness was used to fabricate the cross-section to reinforce the beam. The cross-sectional area of the cold-formed steel was calculated by qualifying the force of mild steel with the force of CFS, as follows:

$$[(253+422.8) * 510] + (157* 450) =$$
Area of the section* 290

$$415308 = 290 \text{ As}$$

Area of cold-formed steel section = 1432.1 mm^2

1432.1 mm² =
$$A_{web} + A_{flange}$$

= $(h*t) + 2*(b*t)$
= $(180*t) + 2(100*t) \rightarrow t= 3.77$ mm